

# USEMA: a Scalable Efficient Mamba Like Attention for Medical Image Segmentation

Elisha Dayag<sup>1</sup>, Nhat Thanh Tran<sup>1</sup>, and Jack Xin<sup>1</sup>

University of California Irvine, Irvine CA 92697

**Abstract.** Accurate medical image segmentation is an integral part of the medical image analysis pipeline that requires the ability to merge local and global information. While vision transformers are able to capture global interactions using vanilla self-attention, their quadratic computational complexity in the input size remains a struggle for medical image segmentation tasks. Motivated by the dispersion property of vanilla self-attention and recent development of Mamba form of attention, Scalable and Efficient Mamba like Attention (SEMA) utilizes token localization via local window attention to avoid dispersion and maintain focusing, complemented by theoretically consistent arithmetic averaging to capture global aspect of attention. In this work, we present USEMA, a hybrid UNet architecture that merges the local feature extraction ability of convolutional neural networks (CNNs) with SEMA attention. We conduct experiments with USEMA across a variety of modalities and image sizes, demonstrating improved computational efficiency compared to transformer based models using full self-attention, and superior segmentation performance relative to purely convolution and Mamba-based models.

**Keywords:** Medical Image Segmentation · Deep Learning · Transformer.

## 1 Introduction

Medical image segmentation is one of the fundamental steps of the medical image analysis pipeline. Accurate segmentation results can assist doctors in providing diagnoses [21]. Medical images present unique challenges in segmentation due to the limited amount of data available for training as well as the complex, overlapping geometry of the objects to be segmented [22].

Inspired by the state of the art performance of Transformer-based frameworks on various computer vision tasks [5], myriad works have studied transformers for medical image segmentation. Many of these works combine utilize hybrid transformer/CNN architectures to utilize the latter’s ability to efficiently extract image features [9, 10, 33]. While vanilla self-attention has a global receptive field and enables a model to capture long-range dependencies, it incurs an  $O(n^2)$  sequence complexity ( $n$  the sequence length) that can be computationally prohibitive. Thus, many works have sought to provide the benefits of attention in a more efficient manner [13, 27, 32].

A recent line of research utilizes state space models like Mamba [6]. These models achieve the global receptive field and dynamic weighting parameters of self-attention with linear time complexity. As of now, multiple papers have been written incorporating Mamba for medical image analysis and demonstrating a marked improvement over the aforementioned attention-based models [17, 28, 30]. At the same time, several studies have utilized aspects of the Mamba architecture to derive efficient attention variants [8, 15, 24]. Some of these Mamba-inspired variants have been utilized in medical image segmentation to great success [12].

In this paper we propose a **UNet** with **Scalable Efficient Mamba-Like Attention** (USEMA). Our model builds upon the SEMA mechanism [24] and utilizes a local-global attention that carefully augments window attention with a theoretically-grounded efficient global attention approximation. By combining this with the adaptive feature selection capabilities of Mamba and integrating the mechanism into a symmetric U-shaped structure, we obtain an architecture that effectively utilizes SEMA’s strengths for the particular task of medical image segmentation. Our results show that USEMA outperforms a number of both Transformer-based and Mamba-based medical image segmentation models across a diverse selection of 2D benchmarks.

## 2 Methods

### 2.1 Preliminary

Transformer [26] has been a dominant architecture in deep learning. The main component is attention mechanism. For given input  $x \in \mathbb{R}^{n \times d}$ , attention is defined as:

$$A(Q, K, V) = \text{softmax}(QK^T)V, \quad (1)$$

where  $Q = xW_Q + b_Q, K = xW_K + b_K, V = xW_V + b_V$ . Here  $W_Q, W_K, W_V \in \mathbb{R}^{d \times d}$  and  $b_Q, b_K, b_V \in \mathbb{R}^{n \times d}$  are learnable parameters. An advantage of the attention mechanism is the ability to select relevant information from the given global context. However, there are two large problems with the use of attention in medical image segmentation. The first and most often referenced is the quadratic computational cost of attention with respect to sequence length [6, 9, 16, 28, 30]. Another issue is that as the sequence length increases, the scores of the attention matrix ( $\text{softmax}((QK^T))$ ) disperse toward 0 uniformly, which hinders the attention’s ability to select important keys and values [24]. To be more precise, under suitable conditions [24] proves that there exists an  $N_0 \in \mathbb{N}$  such that for all  $n > N_0$  we have

$$\frac{C_1}{n} < \text{softmax}((QK^T))_{ij} < \frac{C_2}{n}, \quad (2)$$

for all indices  $0 \leq i, j \leq n$ , and for some  $C_1, C_2 \in \mathbb{R}^+$ . This holds for all attention heads in a transformer. A related probabilistic result also showed [24] that if entries of the attention matrix are random variables allowed to be mildly

correlated, dispersion occurs with high probability as a consequence of the weak law of large numbers.

We can observe experimentally the dispersion phenomenon described theoretically above. We trained UNETR [10], which utilizes full self-attention, on images from the MICCAI 2017 Endovis Challenge [1]. We trained on image patches of size  $1536 \times 896$ , which with the standard  $16 \times 16$  patches of a vision transformer leads to a sequence of length  $96 \times 56 = 5376$ . When we visualize the attention matrices produced by UNETR on test data, as seen in Figure 1, we see that the attention scores are remarkably concentrated around the mean,  $\frac{1}{\text{seq len}}$ .

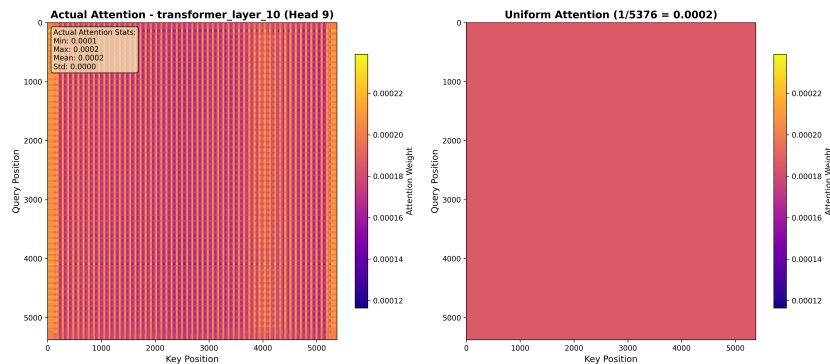


**Fig. 1.** Left: The attention matrix of UNETR on a sequence of length 5376 Right: The attention matrix that would be obtained via a uniform attention i.e. setting each entry to  $1/5376$ . Note that the values in the left-hand matrix are all within  $1e - 4$  of the mean and bounded above by  $2e - 4$  and below by  $1e - 4$ .

A way to mitigate the computational cost is to limit the context window of the selection process, that is window attention defined as:

$$A_w(Q, K, V) := \left[ \frac{\sum_{j \in J(1)} \exp(q_1 k_j^T) v_j}{\sum_{i \in J(1)} \exp(q_1 k_i^T)}, \dots, \frac{\sum_{j \in J(n)} \exp(q_n k_j^T) v_j}{\sum_{i \in J(n)} \exp(q_n k_i^T)} \right]^T, \quad (3)$$

for some index set  $J(m)$ . An example is  $J(m) = \{Mw + 1, \dots, (M + 1)w\}$ , where  $M = \lfloor \frac{m-1}{w} \rfloor$ . This reduces the computational cost to linear with respect to the input sequence length.

As an alternative to window attention, state space models, in particular Mamba, have been a competitive replacement with its linear computational cost [6, 7]. Concretely, Mamba is defined as a map from  $x$  to  $y$  given by the following dynamical equations:

$$h_t = A_t \odot h_{t-1} + B_t(\Delta_t \odot x_t), y_t = C_t h_t + D \odot x_t, \quad (4)$$

where  $x_t, \Delta_t \in \mathbb{R}^{1 \times d}$ ,  $A_t, h_t \in \mathbb{R}^{d \times d}$ ,  $B_t \in \mathbb{R}^{d \times 1}$  and  $y_t \in \mathbb{R}^{1 \times d}$ ,  $C_t \in \mathbb{R}^{1 \times d}$ ,  $D \in \mathbb{R}^{1 \times d}$ , and  $\odot$  denotes the Hadamard product. By induction one can show that



through two branches: in one branch a linear layer followed by SiLU is applied to serve as a gating mechanism similar to Mamba. In the other branch, a linear layer followed by depthwise convolution is applied to the features, followed by the SEMA attention in Eq. (5). Aside from the local-global attention, the features are also enhanced with Rotary Positional Embedding [23] and locally-enhanced position encodings [4]. After undergoing SEMA attention, the two branches are merged via the Hadamard product before being enhanced with another conditional positional encoding to inject spatial position awareness into the post-attention features. Finally the features pass through a feedforward network before moving on to the next block.

In the bottleneck, the spatial dimensions of the image features have been compressed enough so that it is unnecessary computationally to utilize windowed attention. Thus in the bottleneck we use full self-attention.

The decoder consists only of residual blocks and transposed convolutions. As is typical with the UNet structure, we utilize skip connections to connect hierarchical features between the encoder and decoder via concatenation. To produce the segmentation output, we apply a  $1 \times 1$  convolution to the final decoder feature.

### 3 Experiments

#### 3.1 Datasets

To validate the performance of USEMA, we benchmarked it on three datasets spanning multiple imaging modalities, resolutions, and segmentation targets. All of our data preprocessing and loading was done with the nnUNet framework to ensure fair comparisons between our model and benchmarks.

**Abdomen MRI:** This dataset was originally from the MICCAI 2022 AMOS Challenge[19]. It focuses on segmenting 13 abdominal organs from MRI scans, including the liver, right kidney, left kidney, spleen, pancreas, aorta, inferior vena cava, right adrenal gland, left adrenal gland, gallbladder, esophogous, stomach, and duodenum. We followed the settings in [17] and used the original 60 images containing 5615 slices for training and the additional 50 scans containing 3357 slices for testing. We cropped the images into patches of size (320, 320) for training and testing.

**Endoscopy images:** This dataset was originally from the MICCAI 2017 Endovis Challenge [1]. The training and testing data contained image frames from endoscopy videos and the task focused on segmenting seven different instrument types, namely the large needle driver, prograsp forceps, monopolar curved scissors, cadriere forceps, bipolar forceps, vessel sealer, and drop-in ultrasound probe. We followed the official dataset splitting of 1800 images in the training set and 1200 in the test set. In line with other works [16, 17], images were cropped to (384, 640). Notably, this dataset contains a unique aspect ratio compared to the other datasets.

**Microscopy images:** This dataset is from the NeurIPS 2022 Cell Segmentation Challenge [18], which focused on cell segmentation in microscopy images.

It consists of 1000 images for training and 101 images for testing. Unlike the other two datasets, this task is an instance segmentation task. The images in this dataset were cropped to (512, 512).

### 3.2 Implementation Details

To ensure consistency across all datasets, we strictly adhere to the nnUNet-framework [11] for preprocessing. For the microscopy and endoscopy datasets, we used a window size of 16 in our sema block. On the Abdomen MR dataset we used a window size of 32. All other model hyperparameters remained consistent across all datasets. To train our model, we used the AdamW optimizer with learning rate  $3e - 4$  and weight decay 0.05. The loss function is the sum of dice loss and cross-entropy loss and we perform deep supervision [14] at each scale. For each dataset we trained for 1000 epochs using a cosine annealing learning rate scheduler with  $T_{\max} = 100$ .

### 3.3 Benchmarks and Evaluation Details

To assess the performance of our model, we compare it to a variety of transformer-based methods and Mamba-based or Mamba-inspired methods. The transformer-based methods compared against are UNETR, [10], Swin-UNETR [9], and nnFormer [33]. The Mamba-based methods we compare against are U-Mamba [17], Swin-UMamba[16], and Mamba UNet [28]. For U-Mamba, we compare against the variant U-Mamba\_Enc as it is most similar in structure to our USEMA. Similarly for Swin-UMamba, we only compare to the version utilizing the Swin-Umamba encoder.

Dice similarity coefficient (DSC) and normalized surface distance (NSD) were used to evaluate performance on the abdomenMRI and Endoscopy datasets. The microscopy dataset is an instance segmentation task, so we use F1 score for evaluation. We also compute the number of parameters (# param) of each model. Baseline results for DSC, NSD, and F1 score for a number of our models are referenced from [16, 31] except for MLLA-UNet, whose results we report based on their official implementation.

### 3.4 Comparisons on AbdomenMRI Dataset

Table 1 displays the segmentation results on the Abdomen dataset. USEMA outperforms all the comparative baselines, comprising both Mamba-based/inspired and transformer-based methods. In particular, when compared to the other transformer-based methods, our model enhances the DSC and NSD by 5.83% and 4.79% respectively. Additionally, our model is 13% smaller than the best performing transformer-based model. Our model also outperforms all the Mamba-based methods, enhancing the DSC and NSD by 10.53% and 9.60% respectively over the other Mamba-inspired attention variant in MLLA-UNet.

Model	DSC ( $\uparrow$ )	NSD ( $\uparrow$ )	# Params
USEMA (ours)	<b>.7704</b>	<b>.8345</b>	52M
U-Mamba Enc [17]	.7625	.8327	67M
Mamba UNet [28]	.7496	.8178	35M
Swin U-Mamba [16]	.7054	.7647	60M
MLLA-UNet [12]	.6970	.7614	47M
UNETR [10]	.5747	.6309	87M
SwinUNETR [9]	.7028	.7669	25M
nnFormer [33]	.7279	.7963	60M

**Table 1.** Results of organ segmentation on the MICCAI 2022 Abdomen MRI dataset. For a fair comparison, the Swin-UMamba results are reported without the benefit of ImageNet-based pre-training

### 3.5 Comparisons on Endoscopy Dataset

Table 2 shows the segmentation results on the endoscopy dataset. We improve upon the transformer-based methods by 5.63% and 6.31% in DSC and NSD respectively. Our model also outperforms the Mamba-based methods, in particular enhancing the DSC and NSD by 13.49% and 13.51% respectively over the other Mamba-inspired attention variant in MLLA-UNet.

Model	DSC ( $\uparrow$ )	NSD ( $\uparrow$ )	# Params
USEMA (ours)	<b>.6463</b>	<b>.6621</b>	52M
U-Mamba Enc [17]	.6303	.6451	67M
Mamba UNet [28]	.6256	.6370	35M
Swin U-Mamba [16]	.6402	.6547	28M
MLLA-UNet [12]	.5695	.5833	47M
UNETR [10]	.5017	.5168	88M
SwinUNETR [9]	.5528	.5683	25M
nnFormer [33]	.6135	.6228	60M

**Table 2.** Results of instruments segmentation on the Endoscopy 2017 dataset. For a fair comparison, the Swin-UMamba results are reported without the benefit of ImageNet-based pre-training

### 3.6 Comparisons on Microscopy Dataset

Table 3 displays the segmentation results on the microscopy dataset. Compared to the other datasets, this dataset has fewer images, higher image resolution, and larger visual differences. These constraints require the model to capture long-range dependencies and learn in a data efficient manner. We can see that our model outperforms all of the baseline competitors. Among transformer-based models, USEMA enhances the F1 score by 8.61%. USEMA surpasses the other Mamba-inspired architecture MLLA-UNET, by 19.23% in F1 score. Additionally, USEMA manages to have 43% fewer parameters than U-Mamba\_Enc, the strongest Mamba-based model we compared against.

Model	F1 ( $\uparrow$ )	# Params
USEMA (ours)	<b>.5791</b>	52M
U-Mamba Enc [17]	.5607	92M
Mamba UNet [28]	.5215	35M
Swin-UMamba [16]	.5186	60M
MLLA-UNet [12]	.4857	47M
UNETR [10]	.4357	88M
SwinUNETR[9]	.3967	25M
nnFormer [33]	.5332	60M

**Table 3.** Results of cell segmentation on the Microscopy dataset. For a fair comparison, the Swin-UMamba results are reported without the benefit of ImageNet-based pre-training.

## 4 Ablation Study

In this section, we analyze the impact of the global attention approximation in Eq. 5. We retrain USEMA on the same datasets using only the window attention. The results are reported in table 4. We can see that the inclusion of the global attention approximation enhances our models segmentation ability.

Dataset	Model	DSC/F1 ( $\uparrow$ )	NSD ( $\uparrow$ )
Abdomen	USEMA	.7704	.8345
MRI	USEMA w/o attention approx	.7574	.8214
Endoscopy	USEMA	.6463	.6621
	USEMA w/o attention approx	.6218	.6367
Microscopy	USEMA	.5791	–
	USEMA w/o attention approx	.5443	–

**Table 4.** Ablation study of homogeneous mixing (averaging) on the three datasets covered in this paper. In line with the results of Tabs. 1-3 above, we only present F1 score for the microscopy dataset.

## 5 Conclusions

We embedded a mathematically guided scalable and efficient Mamba-like attention (SEMA) in a hybrid Unet architecture to integrate local feature extraction and global information coupling for medical image segmentation. The resulting network USEMA consistently out-performs the state-of-the-art convolution and Mamba (linear time complexity recurrent attention [6]) based models on benchmark abdomen MRI, endoscopy and microscopy images, while saving computational costs compared to transformer based Unet with full attention. In future work, we plan to extend the arithmetic averaging in SEMA to learned and weighted averaging as well as sparsely weighted averaging in case of extremely long tokens, and apply USEMA to large size medical images in pathology [29].

## 6 Acknowledgements

The work was partially supported by NSF grants DMS2219904, DMS-2309520, and a Qualcomm Gift Award. NTT was also funded by a Faculty Endowed Fellowship and the Graduate Scholar Success Fund from UC Irvine.

## References

1. Allan, M., Shvets, A., Kurmann, T., Zhang, Z., Duggal, R., Su, Y.H., Rieke, N., Laina, I., Kalavakonda, N., Bodenstedt, S., et al.: 2017 robotic instrument segmentation challenge. arXiv preprint arXiv:1902.06426 (2019)
2. Ba, J.L., Kiros, J.R., Hinton, G.E.: Layer normalization. arXiv preprint arXiv:1607.06450 (2016)
3. Chu, X., Tian, Z., Zhang, B., Wang, X., Shen, C.: Conditional positional encodings for vision transformers. arXiv preprint arXiv:2102.10882 (2021)
4. Dong, X., Bao, J., Chen, D., Zhang, W., Yu, N., Yuan, L., Chen, D., Guo, B.: Cswin transformer: A general vision transformer backbone with cross-shaped windows. In: Proceedings of the IEEE/CVF conference on computer vision and pattern recognition. pp. 12124–12134 (2022)
5. Dosovitskiy, A.: An image is worth 16x16 words: Transformers for image recognition at scale. arXiv preprint arXiv:2010.11929 (2020)
6. Gu, A., Dao, T.: Mamba: Linear-time sequence modeling with selective state spaces. In: First Conference on Language Modeling (2024), <https://openreview.net/forum?id=tEYskw1VY2>
7. Gu, A., Dao, T., Ermon, S., Rudra, A., Ré, C.: Hippo: Recurrent memory with optimal polynomial projections. In: Larochelle, H., Ranzato, M., Hadsell, R., Balcan, M., Lin, H. (eds.) Advances in Neural Information Processing Systems. vol. 33, pp. 1474–1487. Curran Associates, Inc. (2020)
8. Han, D., Wang, Z., Xia, Z., Han, Y., Pu, Y., Ge, C., Song, J., Song, S., Zheng, B., Huang, G.: Demystify mamba in vision: A linear attention perspective. Advances in neural information processing systems **37**, 127181–127203 (2024)
9. Hatamizadeh, A., Nath, V., Tang, Y., Yang, D., Roth, H.R., Xu, D.: Swin unetr: Swin transformers for semantic segmentation of brain tumors in mri images. In: International MICCAI brainlesion workshop. pp. 272–284. Springer (2021)
10. Hatamizadeh, A., Tang, Y., Nath, V., Yang, D., Myronenko, A., Landman, B., Roth, H.R., Xu, D.: Unetr: Transformers for 3d medical image segmentation. In: Proceedings of the IEEE/CVF winter conference on applications of computer vision. pp. 574–584 (2022)
11. Isensee, F., Jaeger, P.F., Kohl, S.A., Petersen, J., Maier-Hein, K.H.: nnu-net: a self-configuring method for deep learning-based biomedical image segmentation. Nature methods **18**(2), 203–211 (2021)
12. Jiang, Y., Li, Z., Chen, X., Xie, H., Cai, J.: Mlla-unetr: Mamba-like linear attention in an efficient u-shape model for medical image segmentation. arXiv preprint arXiv:2410.23738 (2024)
13. Katharopoulos, A., Vyas, A., Pappas, N., Fleuret, F.: Transformers are rnns: Fast autoregressive transformers with linear attention. In: International conference on machine learning. pp. 5156–5165. PMLR (2020)

14. Lee, C.Y., Xie, S., Gallagher, P., Zhang, Z., Tu, Z.: Deeply-Supervised Nets. In: Lebanon, G., Vishwanathan, S.V.N. (eds.) Proceedings of the Eighteenth International Conference on Artificial Intelligence and Statistics. Proceedings of Machine Learning Research, vol. 38, pp. 562–570. PMLR, San Diego, California, USA (09–12 May 2015), <https://proceedings.mlr.press/v38/lee15a.html>
15. Li, Y., Xie, R., Yang, Z., Sun, X., Li, S., Han, W., Kang, Z., Cheng, Y., Xu, C., Wang, D., et al.: Transmamba: Flexibly switching between transformer and mamba. arXiv preprint arXiv:2503.24067 (2025)
16. Liu, J., Yang, H., Zhou, H.Y., Xi, Y., Yu, L., Li, C., Liang, Y., Shi, G., Yu, Y., Zhang, S., et al.: Swin-umamba: Mamba-based unet with imagenet-based pre-training. In: International conference on medical image computing and computer-assisted intervention. pp. 615–625. Springer (2024)
17. Ma, J., Li, F., Wang, B.: U-mamba: Enhancing long-range dependency for biomedical image segmentation. arXiv preprint arXiv:2401.04722 (2024)
18. Ma, J., Xie, R., Ayyadthury, S., Ge, C., Gupta, A., Gupta, R., Gu, S., Zhang, Y., Lee, G., Kim, J., et al.: The multimodality cell segmentation challenge: toward universal solutions. *Nature methods* **21**(6), 1103–1113 (2024)
19. Ma, J., Zhang, Y., Gu, S., Ge, C., Mae, S., Young, A., Zhu, C., Yang, X., Meng, K., Huang, Z., et al.: Unleashing the strengths of unlabelled data in deep learning-assisted pan-cancer abdominal organ quantification: the flare22 challenge. *The Lancet Digital Health* **6**(11), e815–e826 (2024)
20. Maas, A.L., Hannun, A.Y., Ng, A.Y., et al.: Rectifier nonlinearities improve neural network acoustic models. In: Proc. icml. vol. 30, p. 3. Atlanta, GA (2013)
21. Rayed, M.E., Islam, S.S., Niha, S.I., Jim, J.R., Kabir, M.M., Mridha, M.F.: Deep learning for medical image segmentation: State-of-the-art advancements and challenges. *Informatics in medicine unlocked* **47**, 101504 (2024)
22. Ronneberger, O., Fischer, P., Brox, T.: U-net: Convolutional networks for biomedical image segmentation. In: International Conference on Medical image computing and computer-assisted intervention. pp. 234–241. Springer (2015)
23. Su, J., Ahmed, M., Lu, Y., Pan, S., Bo, W., Liu, Y.: Roformer: Enhanced transformer with rotary position embedding. *Neurocomputing* **568**, 127063 (2024)
24. Tran, N.T., Xue, F., Zhang, S., Lyu, J., Zheng, Y., Qi, Y., Xin, J.: SEMA: a scalable and efficient mamba like attention via token localization and averaging. arXiv:2506.08297, to appear in Intern. Conf. Machine Learning (ICML) 2026.
25. Ulyanov, D., Vedaldi, A., Lempitsky, V.: Instance normalization: The missing ingredient for fast stylization. arXiv preprint arXiv:1607.08022 (2016)
26. Vaswani, A., Shazeer, N., Parmar, N., Uszkoreit, J., Jones, L., Gomez, A., Kaiser, L., Polosukhin, I.: Attention is all you need. *Advances in neural information processing systems* **30** (2017)
27. Wang, S., Li, B.Z., Khabsa, M., Fang, H., Ma, H.: Linformer: Self-attention with linear complexity. arXiv preprint arXiv:2006.04768 (2020)
28. Wang, Z., Zheng, J.Q., Zhang, Y., Cui, G., Li, L.: Mamba-unet: Unet-like pure visual mamba for medical image segmentation. arXiv preprint arXiv:2402.05079 (2024)
29. Wu, H., et al: A whole-slide foundational model for digital pathology from real-world data. *Nature* **630**, 181–188 (2024)
30. Xing, Z., Ye, T., Yang, Y., Cai, D., Gai, B., Wu, X.J., Gao, F., Zhu, L.: Segmamba-v2: Long-range sequential modeling mamba for general 3d medical image segmentation. *IEEE Transactions on Medical Imaging* (2025)

31. Zhang, Z., Ma, Q., Zhang, T., Chen, J., Zheng, H., Gao, W.: Switch-umamba: Dynamic scanning vision mamba unet for medical image segmentation. *Medical Image Analysis* p. 103792 (2025)
32. Zhou, H., Zhang, S., Peng, J., Zhang, S., Li, J., Xiong, H., Zhang, W.: Informer: Beyond efficient transformer for long sequence time-series forecasting. In: *Proceedings of the AAAI conference on artificial intelligence*. vol. 35, pp. 11106–11115 (2021)
33. Zhou, H.Y., Guo, J., Zhang, Y., Han, X., Yu, L., Wang, L., Yu, Y.: nnformer: Volumetric medical image segmentation via a 3d transformer. *IEEE transactions on image processing* **32**, 4036–4045 (2023)